UPPSALA UNIVERSITET

SEGMENTAL AGE DEPENDENCE OF THE RETINAL NERVE FIBRE LAYER CROSS-SECTIONAL AREA AROUND THE OPTIC NERVE HEAD

Philip Strömbäck

Supervisor: Zhaohua Yu
Co-Supervisor: Konstancija Kisonaite

Date: 2024-03-22

Title: SEGMENTAL AGE DEPENDENCE OF THE RETINAL NERVE FIBRE LAYER CROSS-SECTIONAL AREA AROUND THE OPTIC NERVE HEAD

Author: Philip Strömbäck

Table of Contents

1. Populärvetenskaplig sammanfattning (Summary in Swedish)

Glaukom (grön starr) är en progressiv ögonsjukdom som obehandlad kan leda till blindhet. I ögats bakre del finns en öppning, papillen, där nervtrådar från näthinnan lämnar ögat. Efter att nervtrådarna lämnat ögat bildar de synnerven som förser hjärnan med våra synintryck. Vid glaukom skadas näthinnans nervtrådar. Skadorna leder till att nervtrådar förtvinar och slutligen utvecklas synbortfall.

Glaukom är svårdiagnosticerat och sjukdomen upptäcks ofta sent. Skadorna som orsakar synbortfall uppkommer troligen åratal innan synen påverkas. Då patienter oftast söker vård först när synen väl påverkats har redan irreversibla skador uppkommit på nervtrådarna. Dagens metoder för att diagnosticera glaukom upptäcker inte sjukdomen tidigt nog.

Optisk koherenstomografi (OCT) är en icke-invasiv metod som kan avbilda strukturer i ögats bakre del. OCT kan jämföras med ultraljud, men använder ljusvågor i stället för ljudvågor. Med OCT kan tjockleken av nervtrådarna i papillen mätas. Vid glaukom minskar tjockleken eftersom nervtrådarna förtvinar. Genom att mäta denna struktur kan glaukom upptäckas innan synfältet hunnit påverkas.

Nervtrådar förtvinar även vid vanligt åldrande. Det är ännu inte klargjort exakt hur snabbt detta sker för att särskilja en normal åldersbetingad förlust från en sjuklig förlust av nervtrådar.

För att försöka klargöra detta mättes i detta projekt tvärsnittsarean (PIMA) i papillen hos 16 friska individer mellan 30–69 år för att se om det fanns en åldersrelaterad minskning. Detta gjordes i 12 lika stora cirkelsektorer runt papillen för att se om det fanns en skillnad i minskning mellan olika sektorer.

Resultaten visade att en trend till åldersrelaterad minskning kunde ses i den inferior-temporala och temporal-inferiora sektorn. På grund av en liten studiepopulation är resultatet inte statistiskt signifikant och ska tolkas med försiktighet. Fler studier med större studiepopulationer krävs för att med säkerhet kunna säga hur PIMA förändras över tid.

2. Abstract

Background: Glaucoma is a disease which causes a loss of axons in the retinal nerve fibre layer (RNFL) in the optic nerve head (ONH). With optical coherence tomography (OCT), these structures can be objectively quantified. Pigment epithelium Inner limit of the retina Minimal Area (PIMA) is one such parameter, measuring the minimal cross-sectional area of the RNFL in the ONH. As normal reduction of the RNFL occurs over time in healthy individuals, the aim of this project was to determine segmental rate of change for PIMA in non-glaucomatous individuals.

Methods: 16 subjects between ages 30-69 were equally distributed in 4 consecutive age groups. Using Swept-Source (SS)-OCT, 3 volumes were captured in each subject. Two algorithms automatically detected the inner and outer limit of the retina in the ONH, and later calculated PIMA. Linear regression was used to determine age-related loss of PIMA in 12 equally spaced radial segments of the ONH. The same method was used for total PIMA over 2π radians of the ONH. This parameter was named PIMA-2π.

Results: A trend of PIMA loss could be observed in the inferior-temporal and temporal-inferior segments. PIMA-2π was -914.3 ± 9160 μm^2/year (95% confidence interval).

Conclusions: The results were not statistically significant due to large confidence intervals. This was likely due to a small sample size and large inter-individual variation of the parameter. This suggests the best use of the parameter is for comparing one individual against itself over time.

3. Introduction

3.1. Glaucoma

Prevalence

Glaucoma, a disease which is the leading cause of irreversible blindness in the world, is estimated to affect more than 70 million people worldwide.[1] Approximately 10% of the affected population are bilaterally blind.[2] With an aging population worldwide, the number of people with glaucoma is projected to increase to 112 million people by year 2040.[1]

Pathophysiology

Glaucoma can be described as a progressive optic neuropathy, caused by degeneration of retinal ganglion cells (RGCs).[3] The axons of RGCs form the retinal nerve fibre layer (RNFL), the innermost layer of the retina. RGC axons later converge to form the optic nerve, which then exits the eye on its way to the brain.[4]

Degeneration of the retinal ganglion cells results in morphological changes of certain anatomical structures, such as thinning of the retinal nerve fibre layer. With time, degeneration of these cells initially results in peripheral loss of the visual field, as typically seen in individuals with glaucoma.[4]

Risk factors for developing glaucoma include high intraocular pressure (IOP), high age and positive family history of glaucoma.[5] Although high IOP is a risk factor for developing glaucoma, it is not seen in all glaucoma cases.[6]

Methods of Diagnosis

A problem with current methods for glaucoma diagnosis and follow-up is that they do not detect disease early on. An estimated 50% of the glaucoma population remain undiagnosed. Glaucoma is often asymptomatic in the early stage.[7] Subsequently, many patients diagnosed with glaucoma already have irreversible vision loss at time of diagnosis.[8]

Detectable morphological changes of the RNFL precede vision loss. Defects in the RNFL of a glaucoma patient can be found up to 6 years prior to development of the first symptoms.[9] These defects can be assessed with optic nerve head (ONH) and RNFL imaging.[10]

As glaucoma is a progressive disease, early detection of disease progress is key to prevent vision loss.[11] Currently, the gold standard for monitoring progress is repeated automated perimetry, an automated assessment of the patient's visual field. 3 examinations per year during 3-4 years are required in order to accurately detect disease progress in a patient.[12] A limitation with using perimetry is that perimetry measurements suffer from high variability.[13]

Treatment

Glaucoma is incurable. Slowing disease progress and maintaining quality of life is the main objective of glaucoma treatment. The only available treatment involves lowering IOP. This can be done either through pressure-lowering medication, or through surgical intervention.[3]

3.2. Retina and Optic Nerve Head Anatomy

Retina

The retina is comprised of several layers. The innermost layer of the retina is the retinal nerve fibre layer (RNFL). This layer contains the axons of the retinal ganglion cells (RGCs). The RNFL is situated below the internal limiting membrane (ILM), which is connected to the vitreous body. The outermost layer of the retina is the retinal pigmental epithelium layer (RPE). The RPE is connected to the choroid, separated only by a thin membrane called Bruch's membrane.[14]

Optic Nerve Head

Every RGC axon exits the eye through an opening in the sclera. This opening is the site of the optic nerve head (ONH). After leaving the eye, the axons form the optic nerve. The ONH is the site where the RGC axons are most tightly packed.[15] In addition, this is the site where signs of glaucoma first can be noted.[16] The RNFL is thicker in the inferior and superior poles of the ONH.[15]

The ONH varies in size between individuals.[17] With aging, there is a natural reduction of RGCs, and thus a thinning of the RNFL.[18] The normal rate of reduction of the RNFL in the ONH differs depending on what imaging method is used. The rate of change in non-glaucomatous eyes has been found to vary from -0.75 to -1.92 μm/year.[19,20]

3.3. Optical Coherence Tomography

Basic Principle

Optical coherence tomography (OCT) is a high-resolution imaging method by which structures at the back of the eye, such as the retina and the ONH, can be visualised. It is a non-invasive method

that uses the wave-like property of light to visualize a cross-section of the retina. It can be compared to ultrasound, but using light instead of soundwaves.[21]

OCT technology is based on interference. Light is sent out towards the tissue being examined, i.e. the retina. The light passes an interferometer, where part of the light is reflected towards the tissue, and part of the light is reflected towards a reference mirror. Light is reflected back from the tissue and reference mirror, respectively. The two light beams then interfere. Coherent light beams will superimpose and either increase or decrease in amplitude. A photo detector then detects the interference signal, creating a cross-sectional image of the tissue.[22]

Time-Domain OCT

The first OCT technology developed was called Time-Domain OCT (TD-OCT). In TD-OCT the light source is comprised of near-infrared light, and the distance of the reference mirror had to be adjusted manually each scan to correctly identify each layer of the retina.[22] This is time-consuming and can only produce low-resolution two-dimensional visualizations of the retina.[23]

Fourier-Domain OCT

Fourier-Domain OCT (FD-OCT) is a further development of OCT technology. The term FD-OCT comprises both Spectral-Domain OCT (SD-OCT) and Swept-Source OCT (SS-OCT). In SD-OCT, the light source is comprised of broadband light, and the photo detector replaced by a spectrometer.[22] In SS-OCT, the most modern OCT technology, the light source rapidly sweeps across a spectrum of light. The photo detector will register the light spectrum over time.[24]

Both FD-OCT methods produce the final image using Fourier transformation of the registered interference.[22] In addition, the newer methods remove the need for a manually adjusted reference mirror, reducing scan times.[24] FD-OCT methods enable high-resolution images in 3D.[19]

3.4. Clinical Application of OCT

OCT imaging of the retina to measure the RNFL is today routinely used in clinical glaucoma care. This has traditionally been done peripapillary, i.e. not at the ONH.[25] FD-OCT has largely replaced TD-OCT in the clinical setting.[26]

In 2007, Považay et al. suggested quantifying the RNFL thickness in the ONH by measuring the shortest distance between the ILM and the RPE using OCT. This measurement was named minimal circumpapillary band (MCB). MCB was suggested to be a more objective quantification

of the RNFL compared to previous methods, as it would eliminate optic disc tilting as a source of error. In addition, measuring the RNFL at the ONH as compared to peripapillary is thought to be a better representation of actual axon content, as axons are more tightly packed here.[4]

This concept was later expanded on in 2012 by Reis et al. Realising the need for a true anatomical landmark, visible on OCT, for correctly measuring the RNFL in the ONH, they coined the term Bruch's membrane opening-minimum rim width (BMO-MRW). This method measures the shortest distance from the opening of Bruch's membrane to the ILM.[27] BMO-MRW was later used to calculate the cross-sectional area of the RNFL around the ONH, as the term Bruch's membrane opening-minimum rim area (BMO-MRA).[28] It has been suggested that cross-sectional area is a better estimate of actual RGC content than thickness.[29]

Differentiating the BMO from the RPE is not always possible with commercial OCT, due to Bruch's membrane being very thin.[30] Therefore, Sandberg Melin et al. proposed a new nomenclature for measuring the RNFL in the ONH. Here, the thickness of the RNFL is named *Pigment epithelium central limit – Inner limit of the retina Minimal Distance* (PIMD). This distance is measured from the *ONH Pigment epithelium Central Limit* (OPCL) to the *Inner limit of the Retina Closest Point* (IRCP). PIMD can be compared to BMO-MRW.[11]
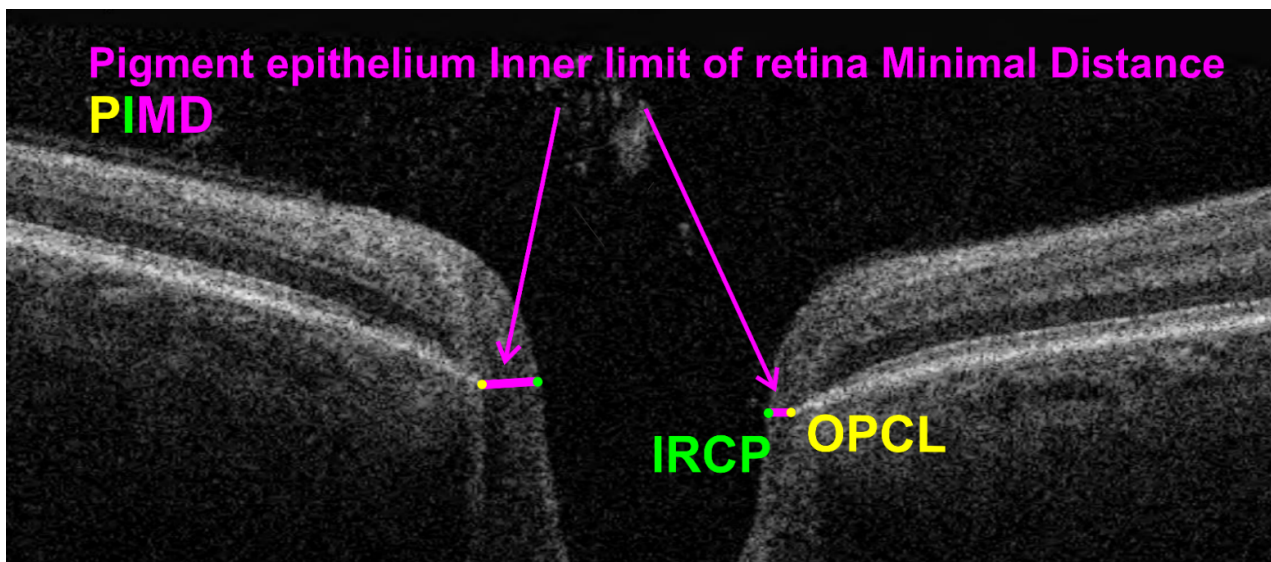
Figure 1. Representation of Pigment epithelium central limit – Inner limit of the retina Minimal Distance (PIMD) as it appears in an OCT scan. PIMD is the distance between ONH Pigment epithelium Central Limit (OPCL) and Inner limit of the Retina Closest Point (IRCP).

As with BMO-MRW, a cross-sectional area measurement has also been developed. For PIMD, this measurement is called *Pigment epithelium Inner limit of the retina Minimal Area* (PIMA).[31] PIMA can be compared to BMO-MRA.
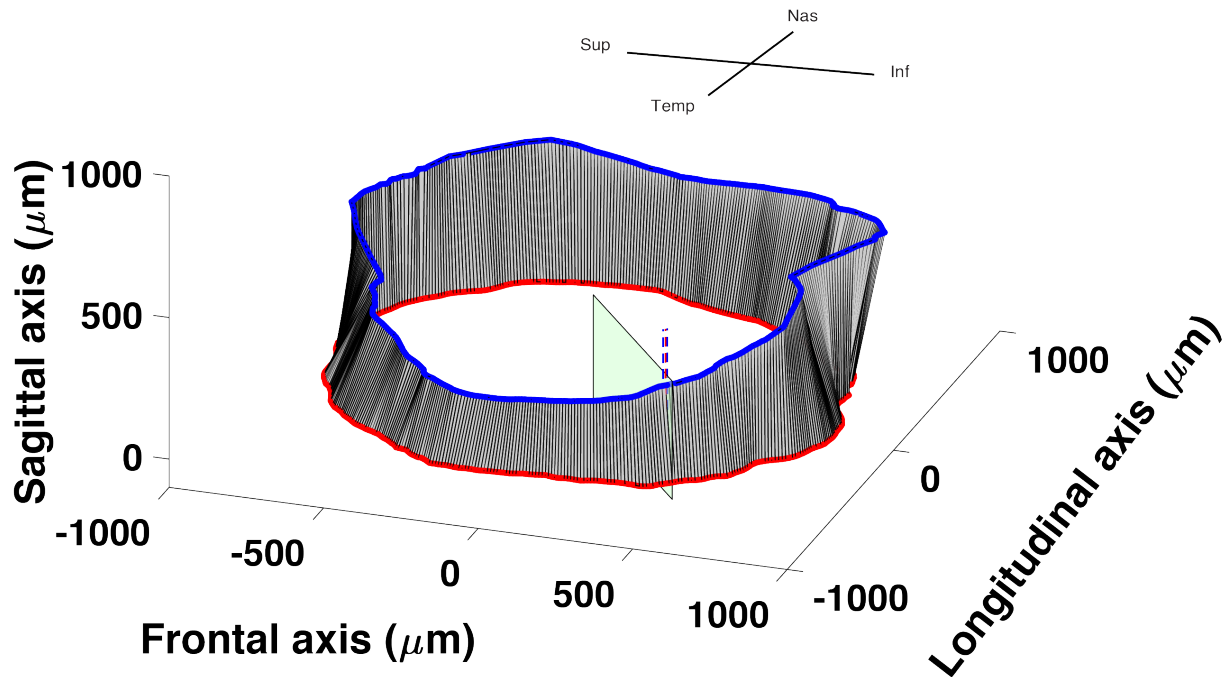
Figure 2. Representation of Pigment epithelium Inner limit of the retina Minimal Area (PIMA) around the total circumference (2π radians) of the ONH.

There is little consensus regarding which method most accurately represents the RNFL in the ONH. It is not fully clear what anatomical structures should be measured in order to most accurately detect glaucomatous damage.[30]

3.5. Artificial Intelligence and Deep Learning in Medical Imaging

Artificial intelligence (AI) is a concept that was introduced in 1956. The concept of AI can be described as devices that are capable of emulating human intelligence.[32] It was Alan Turing that previously had developed the idea of a machine able of displaying human intelligence. In 1950, Turing proposed a method of testing a machine's ability of displaying intelligent behaviour, the Turing test.[33]

Deep Learning (DL) is one form of AI, where a network similar to the human brain enables the technology to learn by experience, rather than having to be programmed. A Convolutional Neural Network (CNN) is a type of DL network designed to process data of several dimensions, such as

data generated by medical imaging.[32] DL algorithms has several applications in ophthalmology, for example automatic detection of structures in OCT volumes.[34]

Previously, only IRCP could be automatically detected by an algorithm. OPCL had to be manually annotated for each of the 500 radial segments. This took on average 7.5 minutes.[11] This process has now been automated, by developing a DL algorithm that automatically detects OPCL, and thus is able to calculate PIMD and PIMA.[35,36]

3.6. Aims

There is a normal age-related thinning of the RNFL.[37] It is not clear at exactly what rate this occur to correctly differentiate normal age-related thinning from glaucomatous damage.[20] This project therefore aims to contribute to determining a reference interval for expected age-related loss of the RNFL in the ONH.

Research Question

Is there age-dependent reduction of the RNFL in the ONH amongst non-glaucomatous individuals?

4. Methods

4.1. Subjects

Subjects were recruited either as volunteers in a non-clinical setting, or amongst patients with an appointment at the Uppsala University Hospital Eye Clinic with no clinical sign of glaucoma as assessed by an ophthalmologist. Inclusion criteria are listed in Table 1. All criteria were self-reported by subjects.

Table 1. Inclusion criteria.

Age [30;69]
Spherical equivalent refractive error [-5;+5] D
No first-degree relative with glaucoma

4.2. Procedure

OCT

Subjects were seated at the OCT. Lights in the room were dimmed. The eye not currently being examined was covered. The chair was locked in place in order to prevent unnecessary movements causing artifacts.

The Macula 3D-Cube, 7x7 mm protocol was selected on the OCT to properly focus the image. After correctly focusing, the Disc 3D-Cube, 6x6 mm protocol was selected for OCT capture.

Three OCT volumes were captured from each eye. Volumes with artifacts were discarded in a later setting. If needed, more volumes were captured until there were at least three volumes of good quality from each eye. This was done at the operator's discretion. All volumes were captured using the same SS-OCT model (OCT Triton, Topcon) and the same operator.

OCT produces a three-dimensional scan of the ONH. The 3D image is comprised of A-scans and B-scans. A-scans are produced by scanning one point in the frontal plane. The OCT moves laterally across the tissue to produce several A-scans. A B-scan is a two-dimensional image comprised of several A-scans at one depth. The 3D image is produced by adding several B-scans together at various depths.

Image Analysis

The 3D image captured by the OCT was exported to a research computer. Two algorithms then calculate PIMD. First, the operator manually selects the centre of the ONH. The Cartesian representation of the ONH is then transformed into polar coordinates around the chosen centre. The first algorithm automatically detects OPCL in 500 equally spaced radial segments around the ONH. The second algorithm automatically detects the ILM. For each of the 500 OPCL points, the closest distance to a point at the ILM is detected. This point is called IRCP. The distance between each OPCL and IRCP point is PIMD.

Subsequently, the minimal cross-sectional area, PIMA, was calculated. For two adjoining OPCL and IRCP points, PIMA is the trapezoidal area limited by these points. This was done for all segments around the ONH. Only data from subjects' right eyes were analysed, as left eye scans contained more artifacts.

4.3. Experimental Design

Subjects were equally distributed into 4 consecutive age groups, [30;39], [40;49], [50;59], [60;69], with an equal number of subjects in each age group.

The 500 radial segments around the ONH were grouped into 12 larger equally sized segments. Starting nasally and counting counter-clockwise, the 12 segments were named as follows: N (nasal), NS (nasal-superior), SN (superior-nasal), S (superior), ST (superior-temporal), TS (temporal-superior), T (temporal), TI (temporal-inferior), IT (inferior-temporal), I (inferior), IN (inferior-nasal), NI (nasal-inferior).

PIMA was calculated for each segment in each subject as the mean of the 3 volumes recorded. In addition, the cross-sectional area around the total circumference of the ONH was calculated as the sum of all segmental areas over 2π radians. This area was named PIMA-2π.
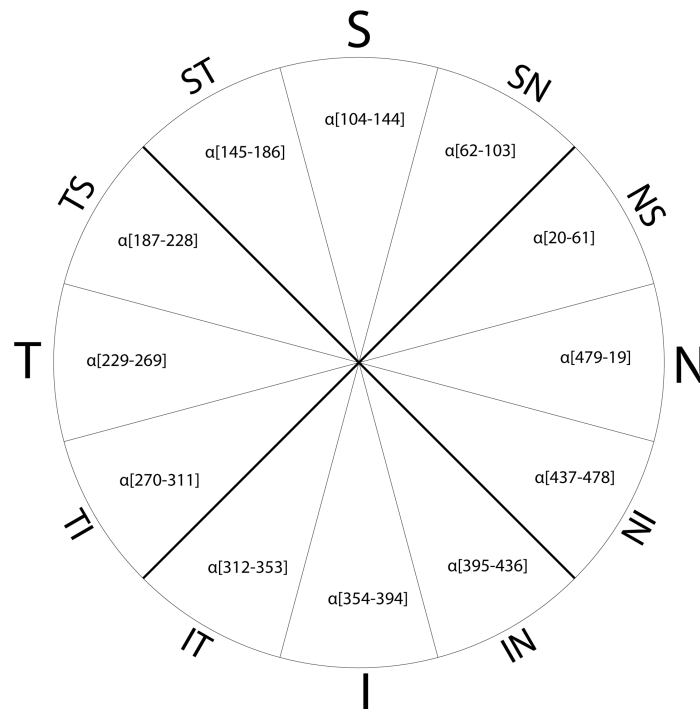
Figure 3. PIMA segments around the ONH: N (nasal), NS (nasal-superior), SN (superior-nasal), S (superior), ST (superior-temporal), TS (temporal-superior), T (temporal), TI (temporal-inferior), IT (inferior-temporal), I (inferior), IN (inferior-nasal), NI (nasal-inferior). The radial segments (1-500) each larger segment contains is written in brackets.

4.4. Statistics

For determining segmental age dependence, PIMA was estimated for each of the 12 segments as a function of age. PIMA-2π was also estimated as a function of age. Regression analysis was used to determine the rate of change of the RNFL. The confidence coefficient was set to 0.95.

4.5. Ethics

This project was part of a larger study with approval from the Swedish Ethical Review Authority (*Etikprövningsmyndigheten*, 2019-05407). Study participants provided their written informed consent in order to participate. All personal data were processed in accordance with the European Union General Data Protection Regulation (GDPR).

5. Results

5.1. Subject Characteristics

In total 20 subjects participated in the project. 4 subjects were later not included in order to have evenly distributed age categories. Of the 16 remaining subjects, there were 6 males and 10 females. Ages ranged from 30 to 68 years. The median age was 48 years. The mean age was 48.75 years.

5.2. Segmental PIMA Rate of Change

A yearly loss of PIMA was seen in 6 of 12 segments (S, TS, T, TI, IT, NI). The largest loss of PIMA was seen in the inferior-temporal segment (IT), with a 95% confidence interval (CI) rate of change of -1033.0 ± 1271 μm^2/year. This was followed by the temporal-inferior (TI) segment with -543.5 ± 861 μm^2/year (95% CI).

Table 2. PIMA yearly rate of change for the 12 radial segments around the ONH.

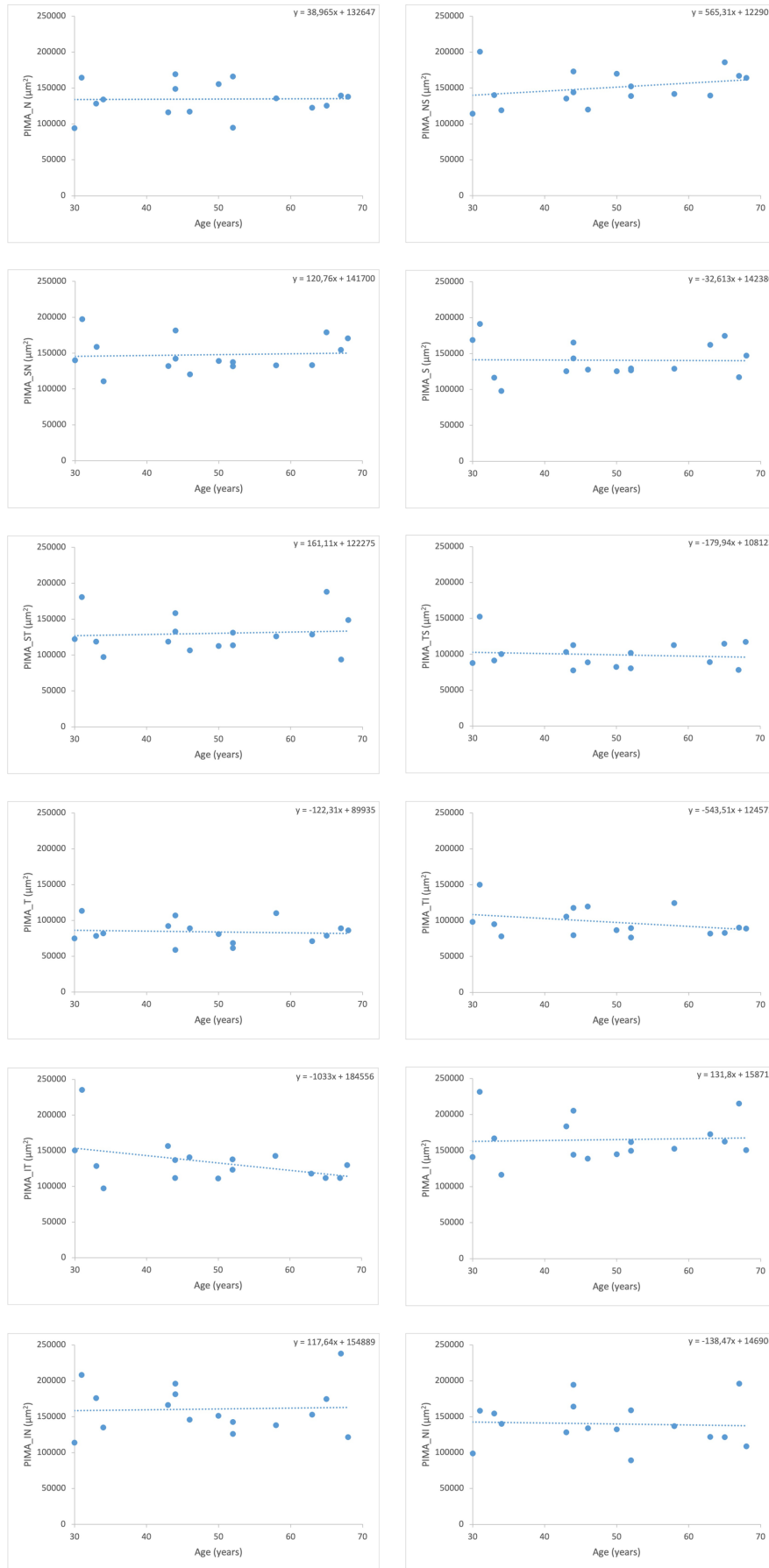| Radial Segment	Rate of Change (μm^2/year) ± 95% CI
1. N (nasal)	39.0 ± 1019
2. NS (nasal-superior)	565.3 ± 1042
3. SN (superior-nasal)	120.8 ± 1061
4. S (superior)	-32.6 ± 1131
5. ST (superior-temporal)	161.1 ± 1195
6. TS (temporal-superior)	-179.9 ± 861
7. T (temporal)	-122.3 ± 712
8. TI (temporal-inferior)	-543.5 ± 861
9. IT (inferior-temporal)	-1033.0 ± 1271
10. I (inferior)	131.8 ± 1360
11. IN (inferior-nasal)	117.6 ± 1500
12. NI (nasal-inferior)	-138.5 ± 1340

Figure 4. Scatter plots of PIMA segments 1-12 as a function of age.

5.3. PIMA-2π Rate of Change

The PIMA-2π, i.e. the minimal cross-sectional area of the RNFL around the total circumference of the ONH, rate of change was -914.3 ± 9160 μm^2/year (95% CI).
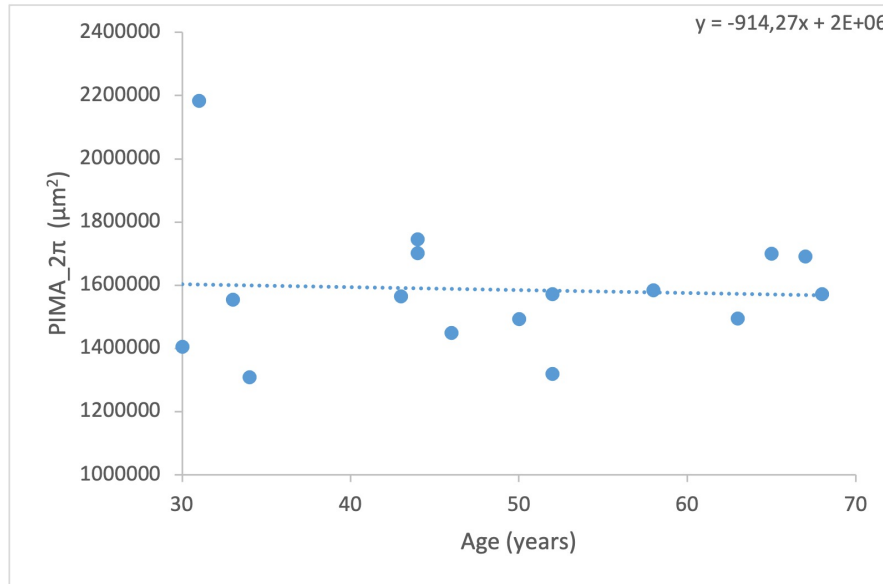
Figure 5. Scatter plot of PIMA-2π as a function of age.

6. Discussion

The aim of this project was to determine segmental PIMA loss rate. A trend of PIMA loss could be observed in the IT and TI segments. However, due to a large confidence interval spanning zero these results are not statistically significant.

It is known that PIMD and other OCT algorithms varies greatly when comparing different individuals, due to variation in the size and shape of the ONH.[38] Variation in an individual is low.[38] This suggests the parameters are better used for detecting changes in an individual over time, rather than comparing an individual to a standardised database of mean population parameters. The large confidence interval seen in this project suggests this also applies for PIMA.

The sample size in this project was small. Originally, 24 subjects were planned to be included. This number was later reduced to 16 due to time constraints. The small sample size is also a reason for the large confidence interval, making it hard to generalise the results.

The subjects in this project were all between ages 30-69. The prevalence of glaucoma increases exponentially with age.[39] Limiting inclusion criteria to a maximum of 69 years limits the generalisability of the project, as normal age-related rate of change needs to be examined for older subjects as well.

Inclusion criteria in this project were all self-reported. Myopia is a factor that can affect OCT parameters.[40] The refractive error reported by subjects in this project was not objectively verified, which is a limitation.

The trend that the IT and TI segments produced the largest PIMA loss (Table 2, Figure 4) should be compared to previous data. A cross-sectional study by Chauhan et al. examining segmental BMO-MRW yearly loss in 246 non-glaucomatous individuals found the largest loss in the inferior segment. There was a large loss observed in the IT segment as well, although not as large as in the inferior segment.[37]

The study by Chauhan et al. used a different OCT algorithm, BMO-MRW, recorded with a different OCT (Spectralis, Heidelberg). BMO-MRW is a one-dimensional parameter, whereas PIMA is a two-dimensional parameter. It used a similar 12-segment representation of the ONH. Comparing the studies is therefore not ideal, but it could be seen as an indication that inferior and

inferior-temporal segments have a greater RNFL loss compared to other segments in non-glaucomatous individuals.

Regarding overall cross-sectional area loss, PIMA-2π loss rate was found to be -914.3 ± 9160 µm^2/year (95% CI, Figure 5). Vianna et al. found the overall yearly BMO area loss in 38 non-glaucomatous individuals to be -3800 µm^2/year.[20] Again, comparing these studies is not ideal. Both parameters are two-dimensional; however, BMO-MRA is calculated as a sum of 48 trapezoidal areas.[28] In contrast, PIMA-2π is calculated as a sum of 500 segments, yielding a higher resolution.[31] This, as well as the difference in sample size, could be seen as reasons to the differences in loss rate.

Using a segmental approach, as done in this project, is a strength. Many OCT imaging methods, both one-dimensional and two-dimensional, produce a measurement as a mean over the total circumference of the ONH. Initial glaucomatous damage often occurs in a small segment of the ONH.[41] A small segmental loss of RGC axons would only cause a small decrease in mean RNFL thickness or area. Dividing the ONH into segments decreases the risk of such a loss going unnoticed.[42] Methods of segmenting the ONH differ.[42] A standardised way of segmenting the ONH should be developed to better compare different OCT algorithms and loss rates in glaucomatous and non-glaucomatous eyes.

Using PIMA, a cross-sectional area parameter, as compared to measuring the RNFL thickness has been suggested to have higher sensitivity for glaucoma detection.[29] The ONH varies in size between individuals.[17] In theory, a larger ONH yields a lower thickness as RGC axons are spread across a wider diameter. A cross-sectional area parameter would be independent of ONH size, producing a more stable parameter with less variability.[31] Another study by Li et al. found BMO-MRW to have higher sensitivity to BMO-MRA, when adjusting for ONH size.[43] More studies with larger sample sizes are needed to fully understand which parameter is the most optimal representation of RGC axon content.

In the future, a much larger sample size is needed to provide a better idea of the normal age-related loss of the RNFL. Even if there is a large variation between individuals, a larger sample size would most likely yield a smaller confidence interval and a more statistically significant result. Older subjects must be included to better represent the population most affected by glaucoma.

7. Conclusion

A trend of PIMA loss could be observed in the IT and TI segments with -1033.0 ± 1271 and 543.5 ± 861 μm^2/year, respectively (95% CI). PIMA-2π loss rate was 914.3 ± 9160 μm^2/year. The results are not statistically significant due to a large confidence interval. The large confidence interval is a likely result of a small sample size and large inter-individual variation of ONH size. Large inter-individual variation of the parameter suggests it should be used for comparing an individual against itself over time.

8. Acknowledgements

9. References

1.	Tham YC, Li X, Wong TY, Quigley HA, Aung T, Cheng CY. Global Prevalence of Glaucoma and Projections of Glaucoma Burden through 2040. *Ophthalmology*. 2014;121(11):2081-2090. doi:10.1016/j.ophtha.2014.05.013

2.	Quigley HA. The number of people with glaucoma worldwide in 2010 and 2020. *British Journal of Ophthalmology*. 2006;90(3):262-267. doi:10.1136/bjo.2005.081224

3.	Weinreb RN, Aung T, Medeiros FA. The Pathophysiology and Treatment of Glaucoma: A Review. *JAMA*. 2014;311(18):1901. doi:10.1001/jama.2014.3192

4.	Považay B, Hofer B, Hermann B, et al. Minimum distance mapping using three-dimensional optical coherence tomography for glaucoma diagnosis. *J Biomed Opt*. 2007;12(4):041204. doi:10.1117/1.2773736

5.	Ekström C. Risk factors for incident open-angle glaucoma: a population-based 20-year follow-up study. *Acta Ophthalmologica*. 2012;90(4):316-321. doi:10.1111/j.1755-3768.2010.01943.x

6.	Karvonen E, Stoor K, Luodonpää M, et al. Prevalence of glaucoma in the Northern Finland Birth Cohort Eye Study. *Acta Ophthalmol*. 2019;97(2):200-207. doi:10.1111/aos.13912

7.	Stein JD, Khawaja AP, Weizer JS. Glaucoma in Adults—Screening, Diagnosis, and Management: A Review. *JAMA*. 2021;325(2):164. doi:10.1001/jama.2020.21899

8.	Weinreb RN, Khaw PT. Primary open-angle glaucoma. *Lancet*. 2004;363(9422):1711-1720. doi:10.1016/S0140-6736(04)16257-0

9.	Sommer A. Clinically Detectable Nerve Fiber Atrophy Precedes the Onset of Glaucomatous Field Loss. *Arch Ophthalmol*. 1991;109(1):77. doi:10.1001/archopht.1991.01080010079037

10.	Michelessi M, Lucenteforte E, Oddone F, et al. Optic nerve head and fibre layer imaging for diagnosing glaucoma. Cochrane Eyes and Vision Group, ed. *Cochrane Database of Systematic Reviews*. 2015;2020(8). doi:10.1002/14651858.CD008803.pub2

11.	Sandberg Melin C, Malmberg F, Söderberg PG. A strategy for OCT estimation of the optic nerve head pigment epithelium central limit-inner limit of the retina minimal distance, PIMD-2π. *Acta Ophthalmol*. 2019;97(2):208-213. doi:10.1111/aos.13908

12.	Chauhan BC, Garway-Heath DF, Goni FJ, et al. Practical recommendations for measuring rates of visual field change in glaucoma. *British Journal of Ophthalmology*. 2008;92(4):569-573. doi:10.1136/bjo.2007.135012

13.	Russell RA, Crabb DP, Malik R, Garway-Heath DF. The Relationship between Variability and Sensitivity in Large-Scale Longitudinal Visual Field Data. *Invest Ophthalmol Vis*

Sci. 2012;53(10):5985. doi:10.1167/iovs.12-10428

14.   Riordan-Eva P, Augsburger JJ, eds. *Vaughan & Asbury's General Ophthalmology, 19e*. 19th ed. McGraw-Hill Education LLC.; 2018.

15.   Dichtl A, Jonas JB, Naumann GOH. Retinal nerve fiber layer thickness in human eyes. *Graefe's Archive for Clinical and Experimental Ophthalmology*. 1999;237(6):474-479. doi:10.1007/s004170050264

16.   Quigley HA, Addicks EM, Green WR, Maumenee AE. Optic nerve damage in human glaucoma. II. The site of injury and susceptibility to damage. *Arch Ophthalmol*. 1981;99(4):635-649. doi:10.1001/archopht.1981.03930010635009

17.   Quigley HA. The Size and Shape of the Optic Disc in Normal Human Eyes. *Arch Ophthalmol*. 1990;108(1):51. doi:10.1001/archopht.1990.01070030057028

18.   Harwerth RS, Wheat JL, Rangaswamy NV. Age-Related Losses of Retinal Ganglion Cells and Axons. *Invest Ophthalmol Vis Sci*. 2008;49(10):4437. doi:10.1167/iovs.08-1753

19.   Tsikata E, Lee R, Shieh E, et al. Comprehensive Three-Dimensional Analysis of the Neuroretinal Rim in Glaucoma Using High-Density Spectral-Domain Optical Coherence Tomography Volume Scans. *Invest Ophthalmol Vis Sci*. 2016;57(13):5498-5508. doi:10.1167/iovs.16-19802

20.   Vianna JR, Danthurebandara VM, Sharpe GP, et al. Importance of Normal Aging in Estimating the Rate of Glaucomatous Neuroretinal Rim and Retinal Nerve Fiber Layer Loss. *Ophthalmology*. 2015;122(12):2392-2398. doi:10.1016/j.ophtha.2015.08.020

21.   Geevarghese A, Wollstein G, Ishikawa H, Schuman JS. Optical Coherence Tomography and Glaucoma. *Annu Rev Vis Sci*. 2021;7:693-726. doi:10.1146/annurev-vision-100419-111350

22.   Aumann S, Donner S, Fischer J, Müller F. Optical Coherence Tomography (OCT): Principle and Technical Realization. In: Bille JF, ed. *High Resolution Imaging in Microscopy and Ophthalmology: New Frontiers in Biomedical Optics*. Springer; 2019. Accessed February 6, 2024. http://www.ncbi.nlm.nih.gov/books/NBK554044/

23.   Sung KR, Kim JS, Wollstein G, Folio L, Kook MS, Schuman JS. Imaging of the retinal nerve fibre layer with spectral domain optical coherence tomography for glaucoma diagnosis. *Br J Ophthalmol*. 2011;95(7):909-914. doi:10.1136/bjo.2010.186924

24.   Husvogt L, Ploner S, Maier A. Optical Coherence Tomography. In: Maier A, Steidl S, Christlein V, Hornegger J, eds. *Medical Imaging Systems: An Introductory Guide*. Springer; 2018. Accessed February 7, 2024. http://www.ncbi.nlm.nih.gov/books/NBK546145/

25.   Wessel JM, Horn FK, Tornow RP, et al. Longitudinal Analysis of Progression in Glaucoma Using Spectral-Domain Optical Coherence Tomography. *Invest Ophthalmol Vis Sci*.

2013;54(5):3613. doi:10.1167/iovs.12-9786

26.   Fan KC, Tsikata E, Khoueir Z, et al. Enhanced Diagnostic Capability for Glaucoma of 3-Dimensional Versus 2-Dimensional Neuroretinal Rim Parameters Using Spectral Domain Optical Coherence Tomography. *Journal of Glaucoma*. 2017;26(5):450-458. doi:10.1097/IJG.0000000000000647

27.   Reis ASC, O'Leary N, Yang H, et al. Influence of Clinically Invisible, but Optical Coherence Tomography Detected, Optic Disc Margin Anatomy on Neuroretinal Rim Evaluation. *Invest Ophthalmol Vis Sci*. 2012;53(4):1852. doi:10.1167/iovs.11-9309

28.   Gardiner SK, Ren R, Yang H, Fortune B, Burgoyne CF, Demirel S. A Method to Estimate the Amount of Neuroretinal Rim Tissue in Glaucoma: Comparison With Current Methods for Measuring Rim Area. *American Journal of Ophthalmology*. 2014;157(3):540-549.e2. doi:10.1016/j.ajo.2013.11.007

29.   Enders P, Adler W, Kiessling D, et al. Evaluation of two-dimensional Bruch's membrane opening minimum rim area for glaucoma diagnostics in a large patient cohort. *Acta Ophthalmologica*. 2019;97(1):60-67. doi:10.1111/aos.13698

30.   Sandberg Melin C. *Morphometry of the Optic Nerve Head as a Diagnostic Tool for Glaucoma*. Acta Universitatis Upsaliensis; 2019.

31.   Kisonaite K, Yu Z, Raeme F, Bendazzoli S, Wang C, Söderberg PG. Automatic estimation of the cross-sectional area of the waist of the nerve fibre layer at the optic nerve head. *Acta Ophthalmologica*. 2024;102(1):91-98. doi:10.1111/aos.15698

32.   Dahrouj M, Miller JB. Artificial Intelligence (AI) and Retinal Optical Coherence Tomography (OCT). *Seminars in Ophthalmology*. 2021;36(4):341-345. doi:10.1080/08820538.2021.1901123

33.   Turing AM. Computing Machinery and Intelligence. *Mind*. 1950;LIX(236):433-460. doi:10.1093/mind/LIX.236.433

34.   Ting DSW, Pasquale LR, Peng L, et al. Artificial intelligence and deep learning in ophthalmology. *Br J Ophthalmol*. 2019;103(2):167-175. doi:10.1136/bjophthalmol-2018-313173

35.   Brusini I, Carizzo G, Bendazzoli S, et al. Fully automatic estimation of the waist of the nerve fiber layer at the optic nerve head angularly resolved. In: Hammer DX, Joos KM, Palanker DV, eds. *Ophthalmic Technologies XXXI*. SPIE; 2021:44. doi:10.1117/12.2583562

36.   Carrizo G, Yu Z, Wang C, Melin CS, Söderberg PG, Kisonaite K. Fully automatic estimation of the angular distribution of the waist of the nerve fiber layer in the optic nerve head. In: Manns F, Söderberg PG, Ho A, eds. *Ophthalmic Technologies XXX*. SPIE; 2020:17. doi:10.1117/12.2554445

37.   Chauhan BC, Danthurebandara VM, Sharpe GP, et al. Bruch's Membrane Opening

Minimum Rim Width and Retinal Nerve Fiber Layer Thickness in a Normal White Population. *Ophthalmology*. 2015;122(9):1786-1794. doi:10.1016/j.ophtha.2015.06.001

38.   Sandberg Melin C, Yu Z, Söderberg PG. Variance components for PIMD-2π estimation of the optic nerve head and consequences in clinical measurements of glaucoma. *Acta Ophthalmol*. 2020;98(2):190-194. doi:10.1111/aos.14197

39.   Quigley HA. Glaucoma. *The Lancet*. 2011;377(9774):1367-1377. doi:10.1016/S0140-6736(10)61423-7

40.   Malik R, Belliveau AC, Sharpe GP, Shuba LM, Chauhan BC, Nicolela MT. Diagnostic Accuracy of Optical Coherence Tomography and Scanning Laser Tomography for Identifying Glaucoma in Myopic Eyes. *Ophthalmology*. 2016;123(6):1181-1189. doi:10.1016/j.ophtha.2016.01.052

41.   Quigley HA, Addicks EM, Green WR. Optic nerve damage in human glaucoma. III. Quantitative correlation of nerve fiber loss and visual field defect in glaucoma, ischemic neuropathy, papilledema, and toxic neuropathy. *Arch Ophthalmol*. 1982;100(1):135-146. doi:10.1001/archopht.1982.01030030137016

42.   Danthurebandara VM, Vianna JR, Sharpe GP, et al. Diagnostic Accuracy of Glaucoma With Sector-Based and a New Total Profile–Based Analysis of Neuroretinal Rim and Retinal Nerve Fiber Layer Thickness. *Invest Ophthalmol Vis Sci*. 2016;57(1):181. doi:10.1167/iovs.15-17820

43.   Li R, Wang X, Wei Y, et al. Diagnostic capability of different morphological parameters for primary open-angle glaucoma in the Chinese population. *BMC Ophthalmol*. 2021;21(1):151. doi:10.1186/s12886-021-01906-6